Journal of Non-Crystalline Solids 358 (2012) 229–235

Contents lists available at SciVerse ScienceDirect

Journal of Non-Crystalline Solids

journal homepage: www.elsevier.com/ locate/ jnoncrysol

Fabrication of mesoporous hydroxycarbonate apatite for oral delivery of poorly water-soluble drug carvedilol

Qinfu Zhao [a], Tianyi Wang [b], Jing Wang [c], Li Zheng [a], Tongying Jiang [a], Gang Cheng [a], Siling Wang [a,*]

[a] Department of Pharmaceutics, School of Pharmacy, Shenyang Pharmaceutical University, No. 103, Wenhua Road, Shenyang 110016, PR China
[b] Department of Clinical Pharmacy, School of Pharmacy, Shenyang Pharmaceutical University, No. 103, Wenhua Road, Shenyang 110016, PR China
[c] Department of Physical Chemistry, School of Pharmacy, Shenyang Pharmaceutical University, No. 103, Wenhua Road, Shenyang 110016, PR China

ARTICLE INFO

Article history:
Received 18 July 2011
Received in revised form 16 September 2011
Available online 12 October 2011

Keywords:
Mesoporous hydroxycarbonate apatite;
Drug delivery system;
Poorly soluble drugs;
Carvedilol

ABSTRACT

The main aim of this study was to prepare nanosized hydroxycarbonate apatite (HCA) as a drug carrier to improve the dissolution rate and increase the bioavailability of poorly soluble drugs, intended to be administered orally. In the present study, uniform mesoporous HCA nanoparticles were synthesized using $CaCO_3$ as a sacrificial template by the hydrothermal method in the presence of cetyltrimethylammonium bromide (CTAB) as a surfactant. The prepared HCA was used as a drug carrier to investigate the drug uptake and release properties employing carvedilol (CAR) as a model drug. The structure and morphology of mesoporous HCA, and the successful storage/release of CAR were systematically studied by N_2 adsorption, scanning electron microscopy (SEM), powder X-Ray diffraction (XRD), differential scanning calorimetry (DSC), thermogravimetric (TG) analysis, Fourier transform infrared (FT-IR) spectroscopy, and UV–VIS spectrophotometry. In vitro drug dissolution tests showed that mesoporous HCA produced burst release of CAR in comparison with micronized CAR in simulated gastric fluid and intestinal fluid. Stability test result indicated that amorphous state of CAR loaded in HCA nanoparticles had a good physical stability after room storage for 6 months. Hence, mesoporous HCA nanoparticles are excellent drug carriers for the oral delivery of poorly soluble drugs.

1. Introduction

The oral delivery is generally regarded as the most acceptable and convenient route [1]. However, about 40% of new chemical entities are insoluble or poorly soluble in water,which may result in incomplete absorption in the gastrointestinal tract[2]. In the Bio-pharmaceutic Classification System (BCS), low solubility and high permeability are the characteristics of BCS Class II poorly water-soluble drugs [3]. The poorly soluble drugs must be dissolved before transmembrane transport. Hence, improving the solubility and dissolution rate is the key to increasing the bioavailability of poorly soluble drugs [4,5]. General methods to improve the solubility and bioavailability of poorly soluble drugs include the use of solid dispersions [6,7], inclusion complexes [8], nanocrystalline [9,10] and liposomes [11]. Recently, mesoporous biomaterials with relatively large surface areas and pore volumes have been widely applied as delivery systems due to their non-toxic and biodegradable properties [12–15].

Apatite is a weak alkaline calcium phosphate-based inorganic compound which has been used as one of the most important artificial bone substitute materials over the past few decades [16]. Most of the synthetic apatite nanoparticles are stoichiometric with a chemical composition of $Ca_{10}(PO_4)_6(OH)_2$. By contrast, the inorganic composition of natural bones is mainly HCA. Hence, synthetic HCA exhibits better biocompatibility and bioactivity than HA [17]. Mesoporous HCA offers several attractive features, such as chemical inertness, high biocompatibility, uniform pore size, and a relatively large surface area, which make it as an excellent candidate for loading poorly soluble drugs. Poorly soluble drugs loaded in mesoporous HCA have a dramatically decreased particle size, increased surface areas and improved wettability. Moreover, poorly soluble drugs in their amorphous state tend to have a higher solubility and dissolution rate, which could markedly improve bioavailability [6, 18]. In view of the above factors, mesoporous HCA has great potential as a drug carrier for oral administration of poorly soluble drugs. However, to our knowledge, the application of mesoporous HCA as a drug delivery system for loading poorly soluble drugs to improve their bioavailability has not yet been documented.

In the present work we develop a simple and new preparation method to produce mesoporous HCA using nanometer-sized calcium carbonate as a sacrificial template by the hydrothermal method in the presence of CTAB as a surfactant. In other words, mesoporous HCA was formed directly from $CaCO_3$ in a phosphate buffer solution via an anion-exchange process [19,20]. The effects of mesoporous HCA on the uptake and release of CAR (Fig. 1) were systematically

* Corresponding author. Tel./fax: +86 24 23986348.
E-mail address: silingwang@syphu.edu.cn (S. Wang).

0022-3093/$ – see front matter © 2011 Elsevier B.V. All rights reserved.
doi:10.1016/j.jnoncrysol.2011.09.020

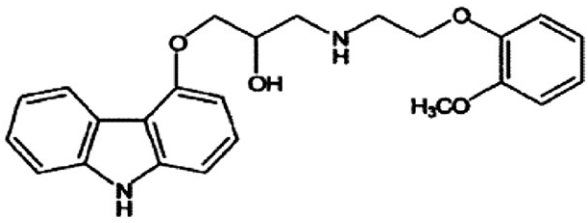

Fig. 1. Molecule structure of CAR.

characterized by N_2 adsorption, SEM, XRD, DSC, TG, FT-IR, and UV–VIS spectrophotometry.

2. Materials and methods

2.1. Materials

Cetyltrimethylammonium bromide (CTAB), disodium hydrogen phosphate ($Na_2HPO_4 \cdot 12H_2O$), hydrochloric acid, potassium dihydrogen phosphate and anhydrous ethanol were purchased from Aladdin (Shanghai, China). All chemicals were analytical grade and used as purchased without further purification. Nanosized calcium carbonate was donated by Jiangxi Huaming Nanometer Calcium Carbonate Co. Ltd. Micronized raw CAR was donated by Shenyang Funing Pharmaceutical Company (Shenyang, China) with a purity>99%. Deionized water was prepared by ion exchange.

2.2. Preparation of mesoporous HCA using $CaCO_3$ as a template

Mesoporous HCA nanoparticles were prepared by an anion-exchange process using calcium carbonate as the sacrificial template and CTAB as a surfactant by the hydrothermal method. In a typical process, 1 g $CaCO_3$ was dispersed in 100 ml mixed solution of anhydrous ethanol and water (volume ratio 1:1) by ultrasound. In addition, the $CaCO_3$ suspensions were further homogenized using an ATS AH100D homogenizer (ATS Engineer Inc, China) at 600 bar for 20 cycles to reduce the aggregation of nanoparticles. Then, 0.3 g or 1 g CTAB and 3.581 g $Na_2HPO_4 \cdot 12H_2O$ were added to the solution under continuous magnetic stirring at 50 °C. The mixed solution was stirred for 1 h before being transferred to a Teflon-lined autoclave for 3 h at 80 °C or 130 °C. The solid precipitates were filtered, washed repeatedly with deionized water and anhydrous ethanol, dried in air at 60 °C for 12 h, and then calcined at 550 °C for 4 h. For simplicity, the HCA nanoparticles synthesized in the present work are referred to as HCA-x-y, e.g., HCA-1 g-80 represents HCA synthesized using 1 g CTAB and a hydrothermal temperature of 80 °C. The parameters of the synthesis experiments are summarized in Table 1.

2.3. CAR-loading procedure

CAR was selected as a model drug because it was practically insoluble in intestinal fluid and water. Mesoporous HCA synthesized using 1 g CTAB at 80 °C had the biggest specific surface area and was selected as the drug carrier. A drug loading process, involving a combination of adsorption equilibrium and solvent evaporation, was employed to increase the drug loading efficiency [21]. Dichloromethane was selected as the loading solvent due to its lower boiling point and its lower toxicity compared with chloroform. Typically, CAR was adsorbed into mesoporous HCA by soaking the HCA nanoparticles in a dichloromethane solution of CAR (40 mg/ml). The mass ratio of carrier to drug in the loading solution ranged from 3:1 to 1:1. Then, the mixture was ultrasonicated for 15 min to ensure that CAR was completely dissolved. Subsequently, the mixture was stirred in a sealed vial for 12 h at room temperature. Finally, the mixture was dried at 50 °C under vacuum for 12 h. The dried drug-loaded sample was referred to as HCA-3-1 (the mass ratio of carrier to drug was 3:1), HCA-2-1 and HCA-1-1, respectively. In comparison, the physical mixture of HCA and CAR (mass ratio was 3:1) was also prepared.

Table 1
Synthetic parameters and nitrogen adsorption parameters of HCA samples and $CaCO_3$.

Sample	The mass of CTAB(g)	Hydrothermal temperature (°C)	Surface area (m^2/g)	Pore volume (cm^3/g)
HCA-0.2 g-80	0.2	80	102.2	0.136
HCA-1 g-80	1	80	121.9	0.175
HCA-0.2 g-130	0.2	130	98.4	0.114
HCA-1 g-130	1	130	118.8	0.135
$CaCO_3$	–	–	25.2	0.047

2.4. Field emission scanning electron microscopy (FE-SEM)

The morphology of the HCA and loaded HCA samples was characterized using an SUPRA 35 field emission scanning electron microscope (ZEISS, Germany). The samples were gold-plated prior to imaging.

2.5. Nitrogen adsorption measurements

SA3100 surface area analyzer (Beckman coulter, USA) was used to measure the N_2 adsorption/desorption isotherms of mesoporous HCA samples at the temperature of (77 K). The surface areas of the samples were calculated using the Brunauer–Emmett–Teller (BET) method from the nitrogen adsorption data over the relative pressure range from 0.05 to 0.2. The pore size distribution was estimated from the adsorption branch of the isotherms using the conventional Barrett–Joyner–Halenda (BJH) method. The total pore volume was determined from the volume adsorbed at a relative pressure of 0.9814.

2.6. Physical state characterization by XRD and DSC

The physical state of CAR in mesoporous HCA was characterized by XRD and DSC. XRD was performed on a diffractometer (PANALY IICALB.V, PW3040/60) with Cu Kα radiation ($\lambda = 1.5405$ Å, 30 kV, 30 mA). Powder samples were scanned over the 2θ angle range from 5° to 60° with a scan rate of 6.0°/min. DSC experiments were performed on a differential scanning calorimeter (DSC 60, Shimadzu Co., Japan). Samples were accurately weighed in aluminum pans and heated at 10 °C/min under a nitrogen flow.

2.7. FT-IR characterization

The FT-IR spectra were recorded on a FT-IR spectrometer (Bruker IFS 55, Switzerland) at room temperature over the spectral region 4000–400 cm^{-1}. All the measurements were performed in a dry atmosphere.

2.8. TG and UV–VIS evaluation of loading efficiency

The drug-loaded HCA samples, blank HCA and pure CAR were analyzed on a TGA-50 instrument (Shimadzu, Japan) to calculate the drug payload efficiency. A sample of about 5 mg was heated from 50 °C to 600 °C at a heating rate of 10 °C/min under N_2 purge of 20 ml/min. About 20 mg of the CAR-loaded samples was dissolved in 20 ml methanol and 80 ml hydrochloric acid (pH 1.2) to determine the drug payload of the HCA carriers. The concentration of CAR in the solution was monitored by UV–VIS spectrophotometry (UV-2000, Unico, USA) at 240 nm after the samples had completely dissolved. The experiments were carried out in triplicate. All experimental data were reported as the mean ± standard deviation.

2.9. Stability test

The sample HCA-3-1 was kept in a desiccator at constant temperature (25 ± 2 °C) for a period of time and characterized by XRD to evaluate the amorphous CAR stability.

2.10. In vitro drug dissolution tests

The in vitro dissolution of CAR was performed in simulated gastric fluid (HCl aqueous solution, pH 1.2) and intestinal fluid (phosphate buffer solution (PBS), pH 6.8). The simulated intestinal juice was prepared using NaOH and KH_2PO_4. Dissolution tests were carried out using the CHP II paddle method (100 ± 1 rpm, 37 ± 0.5 °C and 900 ml dissolution medium) on an RC-8D dissolution tester (Tianjin Guoming Medical Equipment Co., Ltd., China). Samples equivalent to 10 mg CAR were added to the dissolution medium. Aliquots (5 ml) of the release fluid were removed for analysis at predetermined intervals, and replaced immediately with an equal volume of fresh dissolution medium to keep the volume constant. The collected samples were passed through a 0.45 μm membrane filter, and then the concentration of CAR was measured by UV–VIS spectrophotometry at a wavelength of 240 nm. The experiments were carried out in triplicate. All data were expressed as the mean ± standard deviation.

3. Results

3.1. Morphology of synthetic HCA carriers

The influences of factors such as the concentration of CTAB and the hydrothermal temperature have been characterized by SEM and N_2

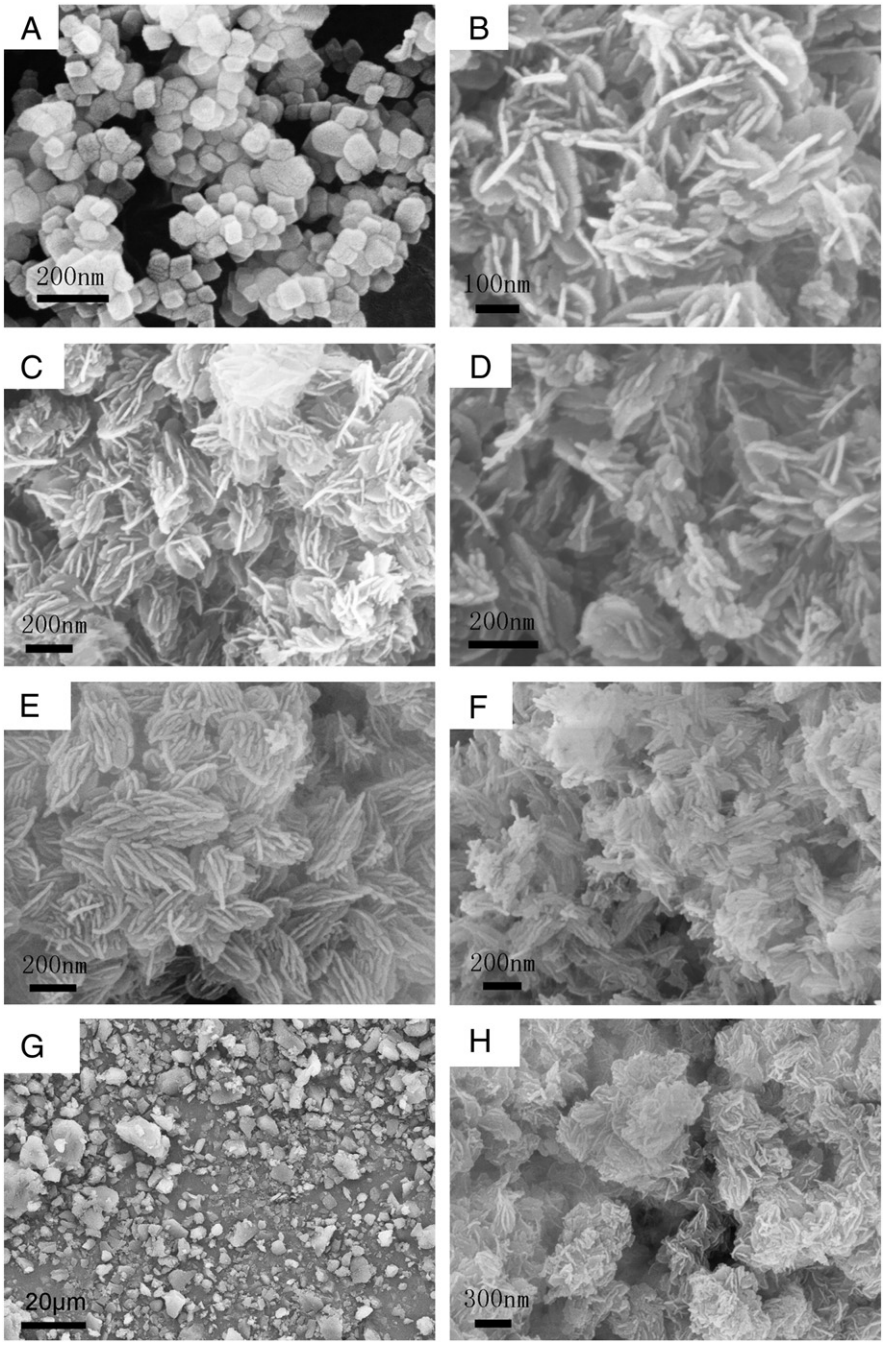

Fig. 2. SEM images of $CaCO_3$ template (A), HCA-1 g-80 (B) and (C), HCA-0.2 g-80 (D), HCA-1 g-130 (E), HCA-0.2 g-130 (F), micronized raw drug (G) and formulation of HCA-3-1 (H).

adsorption. The SEM images of the $CaCO_3$ template and HCA nanoparticles prepared under different conditions are shown in Fig. 2. The $CaCO_3$ nanoparticles had a spherical morphology with an average diameter of about 60 nm. Surprisingly, the morphology of the HCA prepared under different concentrations of CTAB and hydrothermal temperatures was markedly different. The formability of the HCA prepared with 1 g CTAB was better than that of HCA using 0.3 g CTAB under 80 °C according to Fig. 2C and D. The HCA-1 g-80 sample had the shape of a clustered sheet with a thickness of about 15–20 nm. SEM images showed that the shape of HCA synthesized at 130 °C using different concentrations of CTAB were still different (Fig. 2E, F). As shown in Fig. 2G and H, the morphology of the micronized CAR was non-uniform with a diameter ranging from 0.5 to 20 μm, while the morphology of drug loaded HCA nanoparticles was relatively uniform, and no raw drug crystals were present. This result shows that the drug was loaded in the pores or adsorbed on the surface of the carrier which is important for improving the dissolution rate of poorly soluble drugs.

3.2. Estimation of the specific surface area

As presented in Fig. 3, the respective N_2 adsorption isotherms of HCA nanoparticles showed typical type IV curve with a distinct hysteresis loop, indicating the characteristics of mesoporous materials [22,23]. The pore size of mesoporous materials is 2–50 nm. The inset showed that there was only a declining branch above 3.5 nm in the pore size distribution of mesoporous HCA. Although the pore size distribution less than 3.5 nm could not be provided by the SA3100 surface area analyzer, we concluded that the peak of pore size distribution curve was below 3.5 nm. Usually the pore size distributions of mesoporous materials prepared using CTAB as templates are 2–5 nm [24–26], which proved the conclusion that we have inferred. The BET specific surface area (S_{BET}) and total pore volume (V_P) of the HCA samples and $CaCO_3$ are summarized in Table 1. The S_{BET} and V_P of HCA were markedly increased after reacting in PBS compared with $CaCO_3$ nanoparticles. The HCA-1 g-80 sample with the highest S_{BET} of 121.9 m^2/g, and V_P of 0.175 cm^3/g was selected as the drug carrier to investigate the effects on the uptake and release of CAR. The S_{BET} gradually decreased with the incremental drug loading efficiency compared with blank HCA as shown in Table 2, which indicated that CAR was successfully loaded into the mesoporous HCA matrix.

Table 2
S_{BET} and drug loading efficiency before and after CAR uptake.

Sample	Drug loading (%, TGA)	Drug loading (%, UV–vis)	S_{BET} (m^2/g)
HCA-1 g-80	–	–	121.9
HCA-3-1	22.5 ± 1.9	23.6 ± 1.2	56.04
HCA-2-1	31.9 ± 1.4	30.9 ± 1.7	20.55
HCA-1-1	48.7 ± 2.1	48.2 ± 2.3	10.77

3.3. XRD and DSC characterization of CAR-loaded mesoporous HCA

The crystalline properties of CAR, mesoporous HCA, physical mixtures and CAR-loaded HCA samples were evaluated by XRD and DSC. As shown in the XRD patterns (Fig. 4), pure CAR showed intense and characteristic crystalline diffraction peaks at 2θ = 5.8°, 14.9°, 17.5°, 18.4° and 24.3°. The main diffraction peaks of crystalline HCA were clearly seen at 25.8°, 29.4° and 32.0°. However, no distinctive highly crystalline peaks were found in the CAR-loaded HCA samples. The magnified XRD pattern (inset) showed that with an increase in drug loading efficiency (the ratio of carrier: drug decreased from 3:1 to 1:1), the diffraction peaks of CAR become obvious. These results confirmed that the crystalline form of CAR was markedly restricted by the carriers. Also, with the increasing of the proportion of carriers, the degree of inhibition was significantly enhanced.

DSC measurements were performed in order to further verify the physical state of CAR. As shown in Fig. 5, the melting point of crystalline CAR showed a single sharp peak at 117.2 °C. The physical mixture exhibited a slightly wider melting peak than that of crude CAR at 116.0 °C, due to melting of the raw drug. The loaded samples HCA-1-1 and HCA-2-1 exhibited a weaker and wider melting peak than that of the physical mixture with the same ratio. In addition, the melting point of HCA-2-1 was about 5 °C lower than that of the raw drug, which demonstrated a change in the crystal size of the CAR loaded in HCA. No distinct melting peak of CAR was found in the DSC curve of HCA-3-1, which clearly indicated that CAR was in an amorphous state. Accordingly, the DSC results in Fig. 5 confirmed the results obtained by XRD.

3.4. TG and UV–VIS evaluation of drug loading efficiency

TG analysis is an important method for quantifying the amount of loaded drug in inorganic carriers [27]. As presented in Fig. 6,

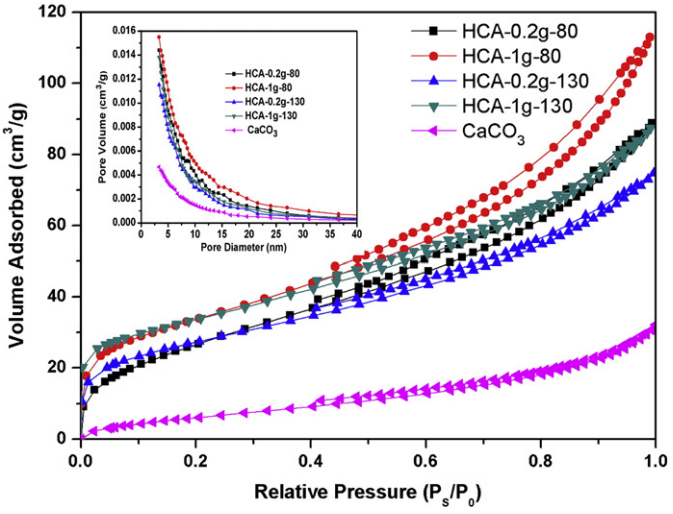

Fig. 3. The nitrogen adsorption/desorption isotherms of prepared HCA samples and $CaCO_3$. The insets show the pore size distributions.

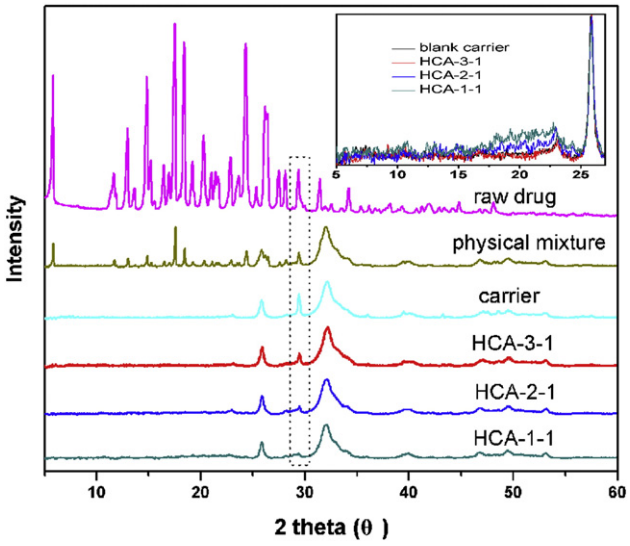

Fig. 4. XRD patterns of raw CAR, blank carrier, physical mixture, HCA-3-1, HCA-2-1 and HCA-1-1.

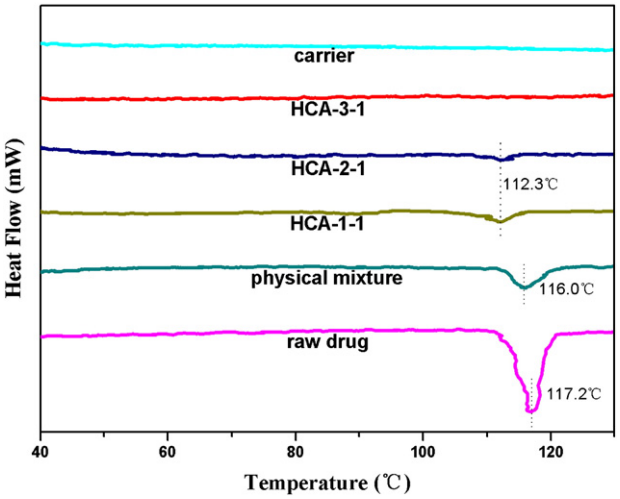

Fig. 5. DSC thermograms of raw CAR, blank carrier, physical mixture, HCA-3-1, HCA-2-1 and HCA-1-1.

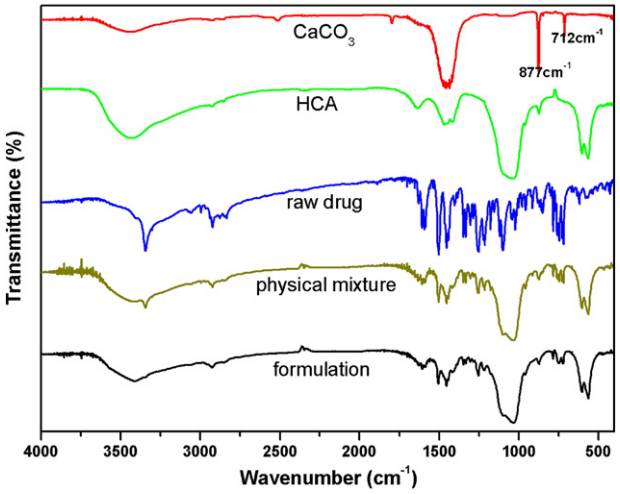

Fig. 7. The FTIR spectra of CAR, pure HA, physical mixture and HCA-3-1.

the percentage of drug loading was calculated from the weight loss between 150 °C and 600 °C relative to the initial weight. According to Fig. 6, the prepared HCA-3-1, HCA-2-1 and HCA-1-1 had a drug uptake efficiency of up to 22.5%, 31.9% and 48.7%, respectively. The drug loading efficiency measured by UV–VIS spectrophotometry agreed with the values determined by TG, as shown in Table 2.

3.5. FT-IR characterization

The FT-IR spectra of template $CaCO_3$, pure HCA, crude CAR, the physical mixture, and the CAR-loaded HCA-3-1 sample are shown in Fig. 7. It has been reported that different $CaCO_3$ polymorphs can be identified by FT-IR spectra. The absorption bands at 565 cm^{-1}, 603 cm^{-1}, and 1038 cm^{-1} corresponded to the PO_4^{3-} group, and the broad absorption band at around 3430 cm^{-1} was attributed to the OH^- group and the clear CO_3^{2-} absorption bands (υ_3) at 1468 cm^{-1} and 876 cm^{-1} indicated that the prepared apatite was HCA. By contrast with blank HCA, raw CAR and the physical mixture, the characteristic peaks of the loaded HCA sample showed no shift, indicating that there was no obvious interaction between HCA and CAR. These results demonstrate that the absorption of CAR loaded in HCA is physisorption.

3.6. Stability test of HCA-3-1 sample

As is well-known to all, the amorphous state of drugs will change to the stable crystalline state under certain conditions. The disadvantage of the amorphous state is its instability during storage. Therefore, the CAR loaded sample HCA-3-1 was characterized by XRD after storage for a period of time to evaluate the physical stability of amorphous CAR. As presented in Fig. 8, no characteristic crystalline peaks of CAR were found in the sample during storage for 6 months. This result indicated that the amorphous state of CAR in HCA had a good physical stability.

3.7. In vitro drug dissolution tests

In vitro dissolution tests were studied in simulated gastric juice and intestinal juice to investigate the dissolution behavior of CAR in different pH conditions. The dissolution profiles of raw CAR and loaded CAR samples in simulated gastric fluid and intestinal fluid are shown in Figs. 9 and 10, respectively. The improved dissolution

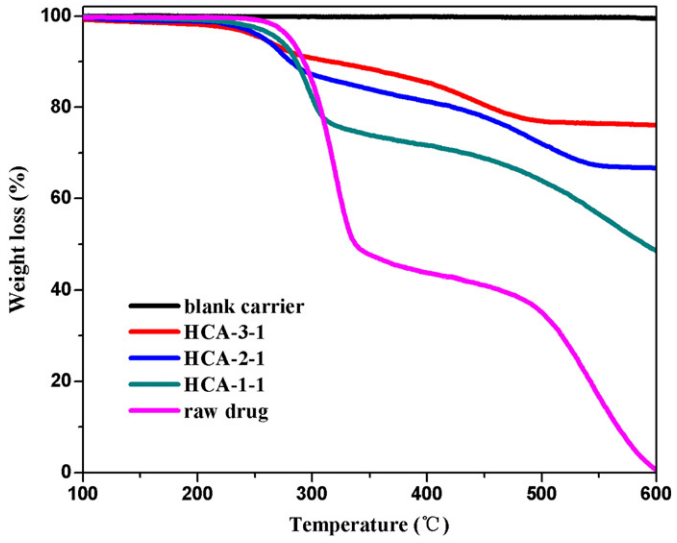

Fig. 6. TG patterns of pure HCA, HCA-3-1, HCA-2-1, HCA-1-1 and CAR.

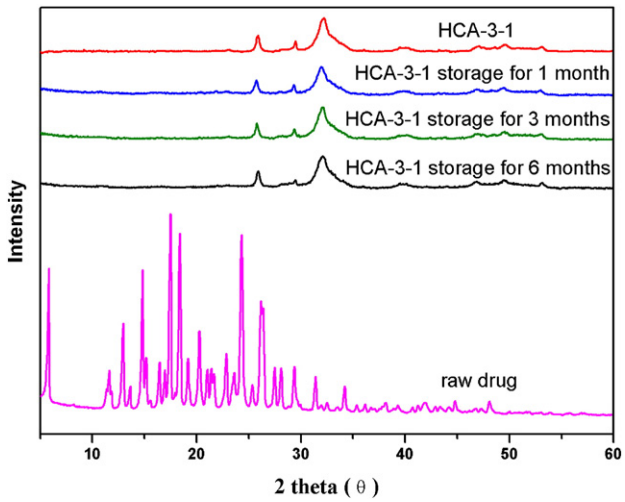

Fig. 8. XRD patterns of HCA-3-1 and pure CAR on different time under storage at room temperature.

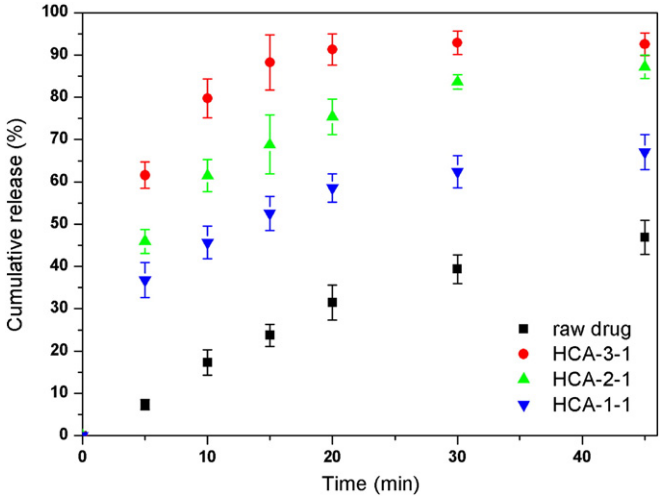

Fig. 9. In vitro drug dissolution profiles of raw CAR, HCA-3-1, HCA-2-1 and HCA-1-1 in simulated gastric fluid (pH 1.2). Each data point represents the mean ± SD of three determinations.

of CAR in simulated gastric fluid was not as significant as in intestinal fluid due to the weak alkaline nature of CAR. As presented in Fig. 9, HCA-3-1 displayed an initial burst release of 60% of CAR during the first 5 min in comparison with less than 10% for raw CAR over the same period. In addition, the cumulative release rate of HCA-3-1 was over 90% within 20 min, while less than 40% of raw CAR had dissolved. A significant improvement in the cumulative release rate of HCA-1-3 in comparison with micronized CAR can be found in Fig. 10. The HCA-3-1 exhibited a fast release of 65% CAR within 20 min, however, raw CAR released more slowly and the released quantity reached only 2%, indicating the poor dissolution rate of the pure CAR in simulated intestinal fluid condition. It was obvious that the loaded HCA samples produced a burst release of CAR compared with micronized CAR in simulated gastric and intestinal fluids. In addition, the cumulative release rate gradually increased with the reduction in drug loading ratio.

4. Discussion

Generally, calcium chloride and calcium nitrate tetrahydrate are used as the calcium sources to synthesize HA nanoparticles. However, calcium carbonate was not only employed as a source of calcium ions, but also used as a template and a source of carbonate ions. The crystal structure of calcium carbonate can be identified by FT-IR spectra. The absorption bands at 877 cm^{-1} (υ_2) and 712 cm^{-1} (υ_4) are attributed to calcite, while the absorption bands at 877 cm^{-1} (υ_2), 744 cm^{-1} (υ_4) are due to vaterite [28]. The appearance of the absorption peaks at 877 cm^{-1} and 713 cm^{-1} clearly indicated that the $CaCO_3$ phase used as a template was calcite (Fig. 7). Usually, ion-exchange reaction was carried out in aqueous solution where a large solubility difference between the salt precursor and the final product [20]. The $CaCO_3$ nanoparticles can be transformed into HCA through ion-exchange due to the driving force of ions replacement—the large solubility difference between HA ($\log K_{sp} = -118.268$) [29] and calcite ($\log K_{sp} = -8.475$) [30]. The calcium ions and carbonate ions were released from $CaCO_3$ nanoparticles and then reacted with phosphate ions spontaneously in the alkaline solution ions according to the following equation.

$$PO_4^{3-} + OH^- + CaCO_3 \rightarrow Ca_{10}[(PO_4), CO_3^{2-}(OH^-)]_6(OH)_2$$

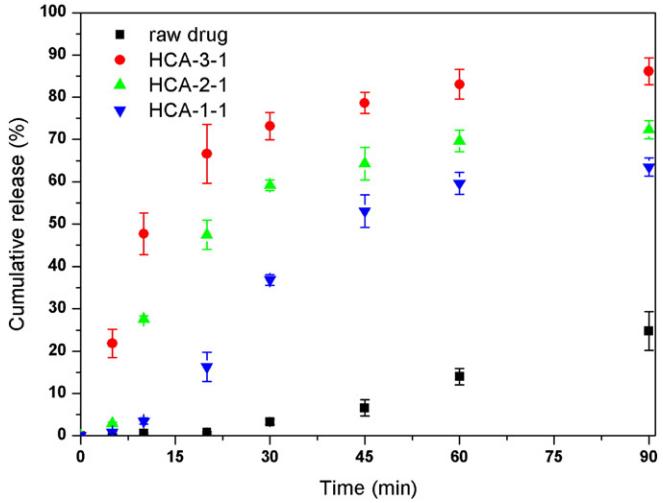

Fig. 10. In vitro drug dissolution profiles of raw CAR, HCA-3-1, HCA-2-1 and HCA-1-1 in simulated intestinal fluid (pH 6.8). Each data point represents the mean ± SD of three determinations.

XRD and DSC results showed that the drug CAR was in an amorphous form loaded in HCA, which might mainly attribute to the inhibition of the pore. This was consistent with results reported in the literature [21,31]. Nano-sized pores limited crystal growth of amorphous drugs. There was not enough space for drug molecules to form long-range order of crystalline structure. Stability tests showed that crystalline form of CAR did not change after storage for 6 months, which could be owing to the recrystallization–inhibition and dispersion effect of the mesoporous HCA. Besides, we found a surprising phenomenon in Fig. 4. With the incremental drug rate in the carriers, the characteristic diffraction peaks of HCA at $2\theta = 29.4°$ gradually weakened. One possible explanation for this was that the characteristic peak of CAR at $2\theta = 29.4°$ coincided with that of HCA, and thus could inhibit the characteristic carrier peak. Furthermore, CAR was in an amorphous state because of the disordered arrangement of the drug molecules. On increasing the drug loaded in the HCA, the disordered arrangement of drug molecules was increased, which might affect the crystal lattice arrangement of HCA.

In vitro dissolution tests showed that mesoporous HCA produced an accelerated release of CAR in comparison with micronized CAR in simulated gastric and intestinal fluids. One major reason for the improved dissolution velocity of CAR may attribute to the solid state of CAR compounds converting from the crystalline state to the amorphous form, which was known to dramatically improve the dissolution rate due to its higher energy state [32]. Nanotechnology has been regarded as an effective method to increase the surface area and reduce drug particle size. According to Noyes–Whitney equation, the increase in surface area and reduction in drug particle size to nanosize range were significant means to improve the dissolution rate of poorly soluble drugs. Furthermore, other factors, such as the better wettability of hydrophilic groups on the surface of HCA and improved dispersibility of CAR after loading in mesoporous HCA matrix, also contributed to the dissolution enhancement.

5. Conclusions

In present work, for the first time, clustered sheet-like HCA nanoparticles were successfully prepared using nanosized calcium carbonate as a sacrificial template with CTAB as a surfactant by hydrothermal method. The prepared HCA nanoparticles had a high S_{BET} and uniform particle size with a drug loading efficiency of up to 22.5%. The successful uptake and release of CAR, which was in an amorphous state, were characterized by N_2 adsorption, SEM, XRD, DSC, FT-IR, TG, and UV–VIS spectrophotometry. In vitro dissolution tests showed that the mesoporous HCA produced an accelerated release of CAR in comparison with micronized CAR in simulated gastric and intestinal

fluids. The enhanced dissolution rate could be largely due to a combination of effects including amorphous state, a clear increase in S_{BET}, a dramatic reduction in particle size and better wettability. The present research demonstrates the great potential of mesoporous HCA as a novel drug carrier for poorly soluble drugs to improve their oral bioavailability.

Acknowledgments

This work was supported by the National Basic Research Program of China (973 Program) (No. 2009CB930300), National Natural Science Foundation of China (No. 81072605), Major National Platform for Innovative Pharmaceuticals (No. 2009ZX09301-012), Key Laboratory of Drug Preparation Design & Evaluation of Liaoning Provincial Education Department and Shenyang special fund for Exploration of Intellectual Resources.

References

[1] F. Kesisoglou, S. Panmai, Y. Wu, Nanosizing— oral formulation development and biopharmaceutical evaluation, Adv. Drug Deliv. Rev. 59 (2007) 631–644.
[2] K. Sachs-Barrable, S.D. Lee, E.K. Wasa, S.J. Thornton, K.M. Wasan, Enhancing drug absorption using lipids: a case study presenting the development and pharmacological evaluation of a novel lipid-based oral amphotericin B formulation for the treatment of systemic fungal infections, Adv. Drug Deliv. Rev. 60 (2008) 692–701.
[3] C. Wu, Z.Y. Wang, Z.Z. Zhi, T.Y. Jiang, J.H. Zhang, et al., Development of biodegradable porous starch foam for improving oral delivery of poorly water soluble drugs, Int. J. Pharm. 403 (2011) 162–169.
[4] C.A. Lipinski, F. Lombardo, B.W. Dominy, P.J. Feeney, Experimental and computational approaches to estimate solubility and permeability in drug discovery and development setting, Adv. Drug Deliv. Rev. 46 (2001) 3–26.
[5] C.A. Lipinski, Poor aqueous solubility — an industry wide problem in drug discovery, Am. Pharm. Rev. 53 (2002) 82–85.
[6] C. Leuner, J. Dressman, Improving drug solubility for oral delivery using solid dispersions, Eur. J. Pharm. Biopharm. 50 (2000) 47–60.
[7] T. Vasconcelos, B. Sarmento, P. Costa, Solid dispersions as strategy to improve oral bioavailability of poor water soluble drugs, Drug Discov. Today 12 (2007) 1068–1075.
[8] S.M. Badr-Eldin, S.A. Elkheshen, M.M. Ghorab, Inclusion complexes of tadalafil with natural and chemically modified b-cyclodextrins I: preparation and in vitro evaluation, Eur. J. Pharm. Biopharm. 70 (2008) 819–827.
[9] E. Merisko-Liversidge, G.G. Liversidge, E.R. Cooper, Nanosizing: a formulation approach for poorly-water-soluble compounds, Eur. J. Pharm. Sci. 18 (2003) 113–120.
[10] C.M. Keck, R.H. Muüller, Drug nanocrystals of poorly soluble drugs produced by high pressure homogenization, Eur. J. Pharm. Biopharm. 62 (2006) 3–16.
[11] A.R. Mohammed, N. Weston, A.G.A. Coombes, M. Fitzgerald, Y. Perrie, Liposome formulation of poorly water soluble drugs: optimisation of drug loading and ESEM analysis of stability, Int. J. Pharm. 285 (2004) 23–34.
[12] Y. Mizushima, T. Ikoma, J. Tanaka, K. Hoshi, T. Ishihara, et al., Injectable porous hydroxyapatite microparticles as a new carrier for protein and lipophilic drugs, J. Control. Release 110 (2005) 260–265.
[13] W. Xia, J. Chang, Well-ordered mesoporous bioactive glasses (MBG): a promising bioactive drug delivery system, J. Control. Release 110 (2006) 522.
[14] F. Ye, H.F. Guo, H.J. Zhang, X.L. He, Polymeric micelle-templated synthesis of hydroxyapatite hollow nanoparticles for a drug delivery system, Acta Biomater. 6 (2010) 2212–2218.
[15] C.M. Zhang, C.X. Li, S.S. Huang, Z.Y. Hou, Z.Y. Cheng, P.P. Yang, C. Peng, J. Lin, Self-activated luminescent and mesoporous strontium hydroxyapatite nanorods for drug delivery, Biomaterials 31 (2010) 3374–3383.
[16] D.M. Dabbs, I.A. Aksay, Self-assembled ceramics produced by complex-fluid templation, Annu. Rev. Phys. Chem. 51 (2000) 601–622.
[17] S.V. Dorozhkin, M. Epple, Biological and medical significance of calcium phosphates, Angew. Chem. Int. Ed. 41 (2002) 3130.
[18] V.B. Pokharkar, L.P. Mandpe, M.N. Padamwar, A.A. Ambike, K.R. Mahadik, A. Paradkar, Development, characterization and stabilization of amorphous form of a low Tg drug, Powder Technol. 167 (2006) 20–25.
[19] Y.P. Guo, Y. Zhou, D.C. Jia, H.X. Tang, Fabrication and characterization of hydroxycarbonate apatite with mesoporous structure, Micropor. Mesopor. Mat. 118 (2009) 480–488.
[20] Y.S. Wang, Y.X. Moo, C.P. Chen, P. Gunawan, R. Xu, Fast precipitation of uniform $CaCO_3$ nanospheres and their transformation to hollow hydroxyapatite nanospheres, J. Colloid Interface Sci. 352 (2010) 393–400.
[21] Y.Z. Zhang, T.Y. Jiang, Q. Zhang, S.L. Wang, Inclusion of telmisartan in mesocellular foam nanoparticles: drug loading and release property, Eur. J. Pharm. Biopharm. 76 (2010) 17–23.
[22] L. Cao, T. Man, M. Kruk, Synthesis of ultra-large-pore SBA-15 silica with two-dimensional hexagonal structure using triisopropylbenzene as micelle expander, Chem. Mater. 21 (2009) 1144–1153.
[23] P. Schmidt-Winkel, W.W. Lukens Jr., D. Zhao, P. Yang, B.F. Chmelka, G.D. Stucky, Mesocellular siliceous foams with uniformly sized cells and windows, J. Am. Chem. Soc. 121 (1999) 254–255.
[24] X.A. Zhang, W.J. Wu, J.F. Wang, X.Z. Tian, Direct synthesis and characterization of highly ordered functional mesoporous silica thin films with high amino-groups content, Appl. Surf. Sci. 254 (2008) 2893–2899.
[25] Q.J. He, X.Z. Cui, F.M. Cui, L.M. Guo, J.L. Shi, Size-controlled synthesis of monodispersed mesoporous silica nano-spheres under a neutral condition, Micropor. Mesopor. Mat. 117 (2009) 609–616.
[26] Z.G. Teng, Y.D. Han, J. Li, F. Yan, W.S. Yang, Preparation of hollow mesoporous silica spheres by a sol–gel/emulsion approach, Micropor. Mesopor. Mat. 127 (2010) 67–72.
[27] J. Salonen, L. Laitinen, A.M. Kaukonen, J. Tuura, M. Björkqvist, et al., Mesoporous silicon microparticles for oral drug delivery: loading and release five model drugs, J. Control. Release 108 (2005) 362–374.
[28] C.M. Li, G.D. Botsaris, D.L. Kaplan, Selective in vitro effect of peptides on calcium carbonate crystallization, Cryst. Growth Des. 2 (2002) 387.
[29] E.C. Moreno, M. Kresak, R.T. Zahradni, Fluoridated hydroxyapatite solubility and caries formation, Nature 247 (1974) 64.
[30] K.J. Westin, A.C. Rasmuson, Nucleation of calcium carbonate in presence of citric acid, DTPA, EDTA and pyromellitic acid, J. Colloid Interface Sci. 282 (2005) 370.
[31] Y.C. Hu, J. Wang, Z.Z. Zhi, T.Y. Jiang, S.L. Wang, Facile synthesis of 3D cubic mesoporous silica microspheres with a controllable pore size and their application for improved delivery of a water-insoluble drug, J. Colloid Interf. Sci. 363 (2011) 410–417.
[32] B.C. Hancock, M. Parks, What is the true solubility advantage for amorphous harmaceuticals? Pharm. Res. 17 (2000) 397–404.